Supplemental Material for: High-Energy Collision of Quarks and Mesons in the Schwinger Model: From Tensor Networks to Circuit QED

Ron Belyansky,[1,2] Seth Whitsitt,[1,2] Niklas Mueller,[3] Ali Fahimniya,[1,2]
Elizabeth Bennewitz,[1,2] Zohreh Davoudi,[4,1] and Alexey V. Gorshkov[1,2]

[1] *Joint Center for Quantum Information and Computer Science, NIST/University of Maryland, College Park, MD 20742 USA*
[2] *Joint Quantum Institute, NIST/University of Maryland, College Park, MD 20742 USA*
[3] *InQubator for Quantum Simulation (IQuS), Department of Physics, University of Washington, Seattle, WA 98195, USA*
[4] *Maryland Center for Fundamental Physics and Department of Physics, University of Maryland, College Park, MD 20742 USA*

(Dated: December 23, 2023)

This Supplemental Material is organized as follows. In Sec. I, we discuss the Thirring-Schwinger model, a generalization of the Schwinger model studied in the main text. In particular, we derive in perturbation theory the effective quark-antiquark Hamiltonian [Eq. (4) of the main text] and discuss the existence (or lack thereof) of bound states. In Sec. II, we derive a corresponding circuit-QED Hamiltonian (including a generalization to 2 dimensions) and discuss an experimental scheme for wave-packet preparation. In Sec. III, we present the details of the numerical tensor-network methods employed, including uniform matrix product states, wave-packet preparation, and particle detection.

CONTENTS

I. THE MASSIVE THIRRING-SCHWINGER MODEL

In this section, we discuss the massive Thirring-Schwinger model, realized in our circuit-QED proposal, including its bosonization, Hamiltonian formulation, and the presence of quark-antiquark bound states for different parameters.

A. Hamiltonian and bosonic dual

Consider the Lagrangian density for the so-called massive Thirring-Schwinger model

$$\mathcal{L} = \bar{\psi}(i\partial\!\!\!/ - eA\!\!\!/ - m)\psi - \frac{1}{4}F_{\mu\nu}F^{\mu\nu} - \frac{1}{2}g(\bar{\psi}\gamma^\mu\psi)(\bar{\psi}\gamma_\mu\psi)\,, \tag{S1}$$

which for $g = 0$ reduces to the massive Schwinger model investigated in this study [Eq. (1) in the main text], while $e = 0$ yields the massive Thirring model [S1, S2]. The gauge fields can be eliminated using Gauss's law [S3], which, after fixing the gauge to $A_1(x) = 0$, reads

$$\partial_x E = -\partial_x^2 A_0 = e\rho, \tag{S2}$$

where $\rho(x) = \psi^\dagger(x)\psi(x)$ is the charge-density operator. The solution to this equation is

$$A_0(x) = a_0 - \frac{e\theta}{2\pi}x - \frac{e}{2}\int dx'\, \rho(x')|x - x'|, \tag{S3}$$

where a_0 and θ are integration constants. As argued in Ref. [S3], physics depends on θ only modulo 2π, and so a suitable range for this variable is $\theta \in (-\pi, \pi]$. The Hamiltonian can be derived in the standard fashion, noting the expression for the electric field from Eq. (S2) with A_0 given in Eq. (S3). In the charge-zero subspace $\int dx\, \rho(x) = 0$, the (normal-ordered) Hamiltonian of the Thirring-Schwinger model becomes

$$\begin{aligned} H = &\int dx\ :\psi^\dagger\gamma^0\left(-i\gamma^1\partial_x + m\right)\psi: - \frac{e^2\theta}{2\pi}\int dx\, x\ :\rho(x): \\ &- \frac{e^2}{4}\int dx \int dx'\, |x - x'|\, :\rho(x)\rho(x'): + \frac{g}{2}\int dx\, :\left[\rho(x)^2 - \left(\psi^\dagger(x)\gamma^0\gamma^1\psi(x)\right)^2\right]. \end{aligned} \tag{S4}$$

Our conventions are such that $\{\gamma^\mu, \gamma^\nu\} = 2\eta^{\mu\nu}$, with metric signature $\eta^{00} = -\eta^{11} = +1$. The two-component spinor operators, $\psi(x,t) \equiv (\psi_1(x,t), \psi_2(x,t))^T$, satisfy the canonical anticommutation relations $\{\psi_a(x,t), \psi_b^\dagger(x',t)\} = \delta_{ab}\delta(x - x')$, where $a, b = 1, 2$. The model described above can be shown to be dual to a bosonic theory with the Hamiltonian [S1–S4]

$$H = \int dx\ :\left[\frac{\Pi^2}{2} + \frac{(\partial_x\phi)^2}{2} + \frac{M^2(\phi + \theta/\beta)^2}{2} - u\cos(\beta\phi)\right]:, \tag{S5}$$

where $[\phi(x), \Pi(y)] = i\delta(x - y)$ and $[\Pi(x), \Pi(y)] = [\phi(x), \phi(y)] = 0$ and the normal-ordering is defined with respect to the boson mass M [S3, S4]. The model parameters are related to those in the fermionic model as follows:

$$M = \frac{e}{\sqrt{\pi}}\frac{1}{\sqrt{1 + g/\pi}}, \quad u = \frac{\exp(\gamma)}{2\pi^{3/2}} m\, e, \quad \beta = \sqrt{\frac{4\pi}{1 + g/\pi}}, \tag{S6}$$

with γ being the Euler's constant. Furthermore, the following relation holds between the fermionic current $\overline{\psi}\gamma^\mu\psi$ and the bosonic field ϕ [S2]:

$$\overline{\psi}\gamma^\mu\psi\ = -\frac{\beta}{2\pi}\epsilon^{\mu\nu}\partial_\nu\phi. \tag{S7}$$

Here, $\epsilon^{\mu\nu}$ is the Levi-Civita tensor. Now, using $\partial_x E = e\overline{\psi}\gamma^0\psi$ [see Eq. (S2)], one arrives at $\frac{e\beta}{2\pi}\phi = E$, which relates the scalar field ϕ to the electric field E. It is more convenient to work with a shifted ϕ: $\phi \to \phi - \theta/\beta$, such that the Hamiltonian is

$$H = \int dx\ :\left[\frac{\Pi^2}{2} + \frac{(\partial_x\phi)^2}{2} + \frac{M^2\phi^2}{2} - u\cos(\beta\phi - \theta)\right]:, \tag{S8}$$

and the relation to the electric field is now $\frac{e\beta}{2\pi}\phi = E + \frac{e\theta}{2\pi} \equiv E_T$, which in the limit $g = 0$ reproduces the relation presented in the main text between the total electric field E_T and the bosonic field of the massive Schwinger model. When $g = 0$, Eq. (S8) reduces to Eq. (2) of the main text.

B. Quark-antiquark interactions and bound states

In this section, we derive an effective quark-antiquark Hamiltonian in the nonrelativistic limit in perturbation theory and use this Hamiltonian to confirm the existence of quark-antiquark bound states (mesons). We also study the meson bound states using nonperturbative tensor-network computation of the low-lying spectrum.

1. *Derivation of effective Hamiltonian*

The goal is to derive an effective interaction Hamiltonian between a quark and an antiquark to leading order in the interactions e and g. For $g = 0$, an analogous computation was discussed by Coleman in Ref. [S3]. The idea is that, in the weak-coupling limit in which $e/m, g \ll 1$, one can restrict the physics to subspaces with fixed particle number, e.g., vacuum, quark-antiquark state, etc. [S5], since transitions between states with different particle numbers are higher order in the coupling strength [S3]. This means that, in this limit, the full Hamiltonian can be assumed to be almost block-diagonal in the Fock basis. This mimics a nonrelativistic limit in which one can define an '*effective*' potential describing interactions in each fixed-particle sector, with well-defined quantum-mechanical operators $\hat{x}$ and $\hat{p}$ which would have been meaningless otherwise. Relativistic corrections in the dynamics can be included using standard quantum-mechanical perturbation theory, while corrections in the kinematics can be included by incorporating higher-order terms in p/m, where p is the typical momentum in the system. Such a notion of an effective Hamiltonian is useful to get a qualitative understanding of the nature of quark-antiparticle interactions in such a limit, and to make analytic predictions for the expected spectrum that can be compared against exact numerics.

To start with, we keep the kinematics relativistic but constrain our analysis to the two-particle sector only. A nonrelativistic expansion in p/m will be performed at the end. First, note that the quadratic piece of the Hamiltonian in Eq. (S4), $H_0 \equiv \int dx \, :\psi^\dagger\gamma^0\left(-i\gamma^1\partial_x + m\right)\psi:$, can be diagonalized by a standard mode expansion:

$$\psi_a(x) = \int \frac{dk}{\sqrt{4\pi E_k}} e^{ikx}\left[u_a(k)b(k) + v_a(-k)c^\dagger(-k)\right], \tag{S9}$$

where $E_k \equiv \sqrt{k^2+m^2}$ with $k \equiv k^1 = -k_1$, and $u(k)$ and $v(k)$ are two-component spinor wave functions that satisfy the classical Dirac equation for positive and negative frequencies, respectively: $(\not{k} - m)u(k) = (\not{k} + m)v(k) = 0$ (here, $\not{k} = E_k\gamma^0 - k\gamma^1$). The creation operators for quarks and antiquarks satisfy the canonical anticommutation relations $\{b(k), b^\dagger(k')\} = \{c(k), c^\dagger(k')\} = \delta(k-k')$. Further, the following representation of Dirac matrices is used for explicit computations, $\gamma^0 = \sigma^z$ and $\gamma^1 = i\sigma^y$, so that the spinor wavefunctions are given by $u(k) = \begin{pmatrix} \sqrt{m+E_k} \\ \frac{k}{\sqrt{m+E_k}} \end{pmatrix}$ and $v(k) = \begin{pmatrix} \frac{k}{\sqrt{m+E_k}} \\ \sqrt{m+E_k} \end{pmatrix}$, leading to the free-fermion Hamiltonian

$$H_0 = \int dk\, E_k\left[b^\dagger(k)b(k) + c^\dagger(k)c(k)\right]. \tag{S10}$$

A quark-antiquark state in the noninteracting limit can be written as

$$|p,q\rangle = b^\dagger(p)c^\dagger(q)|0\rangle, \tag{S11}$$

where $|0\rangle$ is the Fock vaccum of H_0 and where the quark (antiquark) has momentum p (q). Following Coleman [S3], one can now *define* the reduced center-of-mass Hamiltonian as the operator H_{eff}, whose matrix elements in the two-particle sector are given by

$$\langle p', q'|H|p, -p\rangle = \delta(p'+q')\langle p'|H_{\text{eff}}|p\rangle. \tag{S12}$$

The effective Hamiltonian H_{eff} is a function of a conjugate pair of operators $[\hat{x}, \hat{p}] = i$, where $\hat{x}$ is the displacement between the quark and the antiquark and $|p\rangle$ is a single-particle momentum eigenstate, $\hat{p}|p\rangle = p|p\rangle$, with normalization $\langle p'|p\rangle = \delta(p-p')$. In the absence of interactions, one has

$$\langle p', q'|H_0|p, -p\rangle \;= 2\sqrt{m^2+p^2}\,\delta(p-p')\delta(p'+q') \quad \Rightarrow \quad H_{\text{eff}} = 2\sqrt{m^2+\hat{p}^2}\,. \tag{S13}$$

To compute $\langle p', q'|H|p, -p\rangle$ in the interacting case, one can insert Eq. (S9) into Eq. (S4) to obtain

$$\langle p'|H_{\text{eff}}|p\rangle = 2\sqrt{m^2+p^2}\,\delta(p-p') - \frac{e^2\theta}{4\pi^2}\int dx\, x\, e^{i(p-p')x} + \frac{e^2}{8\pi E_{p'}E_p}\left(m^2 + p'p + E_{p'}E_p\right)\int dx\,|x|\,e^{i(p-p')x}$$

$$+ \frac{e^2}{8\pi}\frac{m^2}{E_{p'}^2E_p^2} - \frac{g}{2\pi E_{p'}E_p}\left(m^2 + p'p + E_{p'}E_p\right). \tag{S14}$$

Note that all interaction terms are of the form

$$\langle p'|\hat{O}|p\rangle = f_1(p')f_2(p)\int\frac{dx}{2\pi}\,g(x)\,e^{i(p-p')x} \tag{S15}$$

for some functions f_1, f_2, and g [for the last line of Eq. (S14), $g(x)=\delta(x)$]. This allows any interaction term $\hat{O}$ to be written as follows:

$$\begin{aligned}
\hat{O} &= \left(\int dp'\,|p'\rangle\langle p'|\right)\hat{O}\left(\int dp\,|p\rangle\langle p|\right)\\
&= \int dp'\int dp\,|p'\rangle f_1(p')f_2(p)\int\frac{dx}{2\pi}\,g(x)\,e^{i(p-p')x}\langle p|\\
&= f_1(\hat{p})\int dp'\int dp\,|p'\rangle\left(\int dx\,g(x)\langle p'|x\rangle\langle x|p\rangle\right)\langle p|f_2(\hat{p})\\
&= f_1(\hat{p})\left(\int dp'\,|p'\rangle\langle p'|\right)g(\hat{x})\left(\int dx\,|x\rangle\langle x|\right)\left(\int dp\,|p\rangle\langle p|\right)f_2(\hat{p})\\
&= f_1(\hat{p})g(\hat{x})f_2(\hat{p})\,.
\end{aligned} \tag{S16}$$

Equation (S15) is used in the second equality, and the identity $e^{i(p-p')x}=2\pi\langle p'|x\rangle\langle x|p\rangle$ is used in the third equality. Finally, the effective Hamiltonian can be written as

$$\begin{aligned}
H_{\text{eff}} &= 2\left(m^2+\hat{p}^2\right)^{1/2} - \frac{e^2\theta}{2\pi}\hat{x} + \frac{e^2}{4}\frac{m}{m^2+\hat{p}^2}\delta(\hat{x})\frac{m}{m^2+\hat{p}^2}\\
&+\frac{e^2}{4}\left[|\hat{x}| + \frac{\hat{p}}{(m^2+\hat{p}^2)^{1/2}}|\hat{x}|\frac{\hat{p}}{(m^2+\hat{p}^2)^{1/2}} + \frac{m}{(m^2+\hat{p}^2)^{1/2}}|\hat{x}|\frac{m}{(m^2+\hat{p}^2)^{1/2}}\right]\\
&-g\left[\delta(\hat{x}) + \frac{\hat{p}}{(m^2+\hat{p}^2)^{1/2}}\delta(\hat{x})\frac{\hat{p}}{(m^2+\hat{p}^2)^{1/2}} + \frac{m}{(m^2+\hat{p}^2)^{1/2}}\delta(\hat{x})\frac{m}{(m^2+\hat{p}^2)^{1/2}}\right].
\end{aligned} \tag{S17}$$

The lengthy expression in Eq. (S17) can be simplified by considering the nonrelativistic limit. Note that, when momentum and energy are large enough for particle creation, $\langle\hat{p}^2\rangle \gtrsim m^2$, non-particle-conserving, i.e., inelastic, transitions can occur, and, in such a regime, it is not particularly useful to consider an effective potential between a quark and an antiquark. However, since our interest is in an effective interaction between static or slow-moving quark and antiquark—in particular, for investigating the presence of bound states—the matrix elements between states with different particle numbers will be reduced by kinematic constraints. Note that this limit is only applicable when the dimensionless coupling constants e/m and g are small enough, since large couplings result in binding- or scattering-energy scales large enough to violate these assumptions. Based on this discussion, H_{eff} can be expanded in $p/m \ll 1$ to obtain a simpler effective Hamiltonian at leading order in p/m, e/m, and g:

$$H_{\text{eff}} = 2m + \frac{\hat{p}^2}{m} + \frac{e^2}{2}\left(|\hat{x}| - \frac{\theta}{\pi}\hat{x}\right) + \frac{e^2}{4m^2}\delta(\hat{x}) - 2g\delta(\hat{x}). \tag{S18}$$

In taking the large-m limit, the dimensionless combination e/m is kept fixed. For the Schwinger model, $g=0$, this gives Eq. (4) in the main text. Note that the electric ($e\neq 0$) and the Thirring ($g\neq 0$) interactions contribute short-range terms which compete with each other. In the confined phase ($\theta\neq\pi$), the linear potential guarantees quark-antiquark bound states, which are the fundamental excitations, regardless of the short-range interactions. However, in the deconfined phase ($\theta=\pi$), quarks are free particles (as long as $x>0$, i.e., the quark is to the left of the antiquark). Here, the presence of bound states depends on the delta-function term in Eq. (S18). When $g>g_c\equiv\frac{e^2}{8m^2}$, the delta-function term is negative, giving rise to attractive short-range interactions, implying the existence of at least one bound state. For $g<g_c$ (including the $g=0$ case considered in the main text), on the other hand, the delta function is repulsive, prohibiting any bound states from forming.

As a nontrivial check on this expression, consider the Thirring model, $e = 0$, which is an integrable quantum field theory whose spectrum is known exactly [S6, S7]. The effective Hamiltonian in this case is simply

$$H_{\text{eff}} = 2m + \frac{\hat{p}^2}{m} - 2g\delta(\hat{x})\,. \tag{S19}$$

This is a standard problem in introductory quantum mechanics (see e.g., Ref. [S8]). For $g > 0$, there is a single bound state with energy

$$E_{\text{bound}} = 2m\big(1 - \frac{g^2}{2}\big). \tag{S20}$$

The exact Thirring model with $g > 0$ has N bound states, where N is the largest integer smaller than $1 + 2g/\pi$, and the energy of the nth bound state is given by [S6]

$$E_n = 2m \sin\left(\frac{n\pi/2}{1 + 2g/\pi}\right), \quad n = 1, 2, .., N\,. \tag{S21}$$

For small g, there is a single bound state ($n = 1$) with energy given, at leading order in g, by Eq. (S20).

2. *Numerical verification*

To go beyond the perturbative results, we make use of the variational uMPS quasiparticle ansatz [see Sec. III A and Eq. (S38)] to verify the existence of the bound states. In the deconfined phase, quarks are topological "kinks" [S3], and are numerically described by the topological uMPS ansatz, whereas the mesons, if they exist, would be described by the topologically trivial uMPS ansatz (see Sec. III). The energy minimization of the topological uMPS ansatz yields the quark mass m_q, and the minimization of the topologically trivial uMPS ansatz returns an energy which we denote m_π. To determine if this corresponds to a meson eigenstate, we plot the ratio m_π/m_q in Fig. S1 as a function of g. If the meson exists, that ratio needs to satisfy $m_\pi/m_q < 2$, since the bound-state energy must be below the two-particle continuum beginning at $2m_q$. Furthermore, plotting this ratio for different values of the bond dimension D of the uMPS ansatz can signify the existence or absence of the meson. This is because, if the meson exists, its wavefunction will be localized, and so the ansatz energy m_π should be rather insensitive to D and will quickly converge to the true meson mass as D is increased [S9].

Figure S1 reveals a critical $g_c \approx 1$ (for the parameters used in the main text) above which $m_\pi/m_q < 2$. This region clearly shows insensitivity to D, signaling that the ansatz properly captures the nature of the bound-state wave

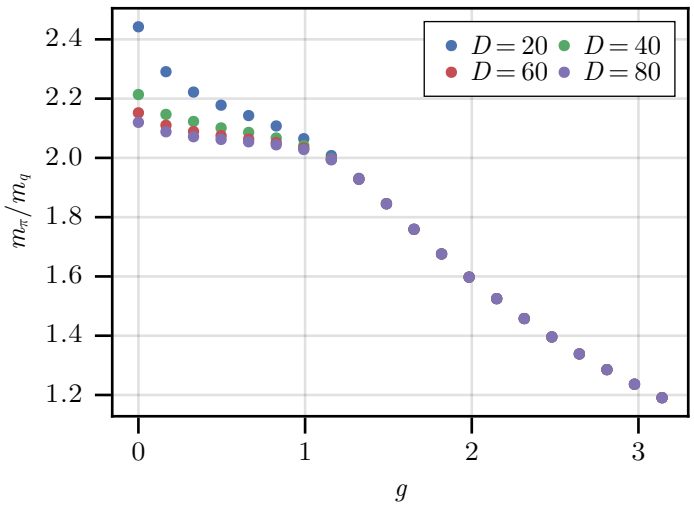

FIG. S1. Ratio of the meson mass m_π to the quark mass m_q in the deconfined phase ($\theta = \pi$) as a function of the Thirring interaction strength g, for different bond dimensions D. The energies are calculated using the variational principle with the uMPS quasiparticle ansatz [see Eq. (S38)] using the same parameters as in the main text ($\chi = 1, \mu^2 = 0.5$, and $\lambda = 0.1$).

function even for smaller bond dimensions. Below g_c, on the other hand, $m_\pi/m_q > 2$, and a qualitatively different behavior is observed as a function of D, signaling sensitivity to the choice of bond dimension. All this suggests that the bound state in the deconfined phase only exists for sufficiently large g, in agreement with the analytical prediction in the previous section. In the absence of a bound state excitation, the minimization of the topologically trivial uMPS ansatz can only yield a multi-particle state that is not an eigenstate, but is rather a superposition of many eigenstates from the multi-particle continuum. Increasing the bond dimension of such a state leads to a reorganization of the particles in it and a reduction of their interaction energy, giving rise to a strong dependence of the state energy on the bond dimension, as can be seen in Fig. S1.

II. CIRCUIT-QED IMPLEMENTATION

In this section, we derive the circuit-QED Hamiltonian from a lumped-element model and present a scheme for preparing meson excitations.

A. Hamiltonian derivation

Consider the circuit diagram in Fig. S2, which is a more detailed version of Fig. 4 of the main text. Here, each unit cell consists of a capacitor with capacitance C, an inductor with inductance L, and a Josephson junction with critical current I_c, in parallel, representing a general rf-SQUID circuit, which includes the fluxonium as a special case [S10]. Each L-J loop is threaded by an external flux Φ_{ext}, and different unit cells are coupled together via inductors with inductance L'. Node fluxes are labeled by ϕ_i, branch fluxes by ϕ_C^i, ϕ_J^i, and ϕ_L^i, for the corresponding elements within node i, and the inter-node branch fluxes coupling nodes i and $i+1$ by $\phi_{L'}^{i,i+i}$. The branch currents are related to the branch fluxes by $I_C^i = C\ddot{\phi}_i$, $I_L^i = \phi_L^i/L$, $I_{L'}^{i,i+1} = \phi_{L'}^{i,i+1}/L'$, and $I_J^i = I_c \sin\left(\phi_J^i\right)$, for the capacitor, inductors, and the Josephson junction, respectively [S11].

The Hamiltonian of the circuit can be derived by standard means. The capacitor branch fluxes are chosen to be equal to the node fluxes $\phi_C^i = \phi_i \,\forall\, i$. Flux quantization yields the remaining branch fluxes: $\phi_J^i + \phi_C^i = \Phi_{\text{ext}}$, $\phi_C^i + \phi_L^i = 0$, $\phi_J^{i-1} + \phi_C^i + \phi_{L'}^{i-1,i} = 0$. Current conservation gives $I_{L'}^{i-1,i} - I_C^i + I_L^i + I_J^i - I_{L'}^{i,i+1} = 0$, which, together with the above, yields the equation of motion

$$-C\ddot{\phi}_i - \frac{1}{L}\phi_i + I_c \sin(\Phi_{\text{ext}} - \phi_i) + \frac{1}{L'}(\phi_{i-1} - 2\phi_i + \phi_{i+1}) = 0. \tag{S22}$$

The corresponding Lagrangian is

$$\mathcal{L} = \sum_i \left[\frac{C\dot{\phi}_i^2}{2} - \frac{(\phi_i - \phi_{i-1})^2}{2L'} - \frac{\phi_i^2}{2L} - I_c \cos(\phi_i - \Phi_{\text{ext}})\right]. \tag{S23}$$

Defining the conjugate momentum $\pi_i = \frac{\partial \mathcal{L}}{\partial \dot{\phi}_i} = C\dot{\phi}_i$ and imposing the canonical commutation relations $[\phi_i, \pi_j] = i\delta_{ij}$, we obtain the Hamiltonian

$$H = \sum_i \left[4E_C\pi_i^2 + \frac{E_{L'}(\phi_i - \phi_{i-1})^2}{2} + \frac{E_L\phi_i^2}{2} + E_J\cos(\phi_i - \Phi_{\text{ext}})\right], \tag{S24}$$

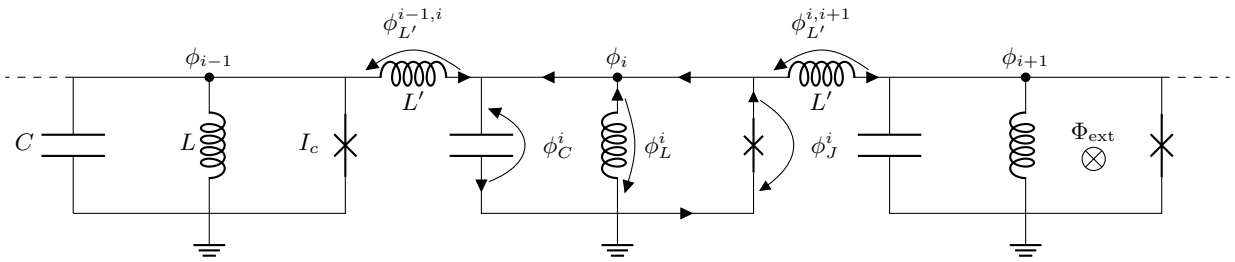

FIG. S2. Circuit diagram implementing the massive Thirring-Schwinger model. An external flux Φ_{ext} threads each L-J loop.

where we defined the energies

$$E_C = \frac{1}{8C}, \quad E_{L'} = \frac{1}{L'}, \quad E_L = \frac{1}{L}, \quad I_J = E_J. \tag{S25}$$

Redefining $\phi_i \to \beta\phi_i$ and $\pi_i \to \pi_i/\beta$, we obtain

$$H = \chi \sum_i \left[\frac{\pi_i^2}{2} + \frac{(\phi_i - \phi_{i-1})^2}{2} + \frac{\mu^2 \phi_i^2}{2} - \lambda \cos(\beta\phi_i - \theta) \right], \tag{S26}$$

which is Eq. (3) of the main text with

$$\chi = \frac{8E_C}{\beta^2}, \quad \frac{E_{L'}\beta^4}{8E_C} = 1, \quad \mu^2 = \frac{E_L\beta^4}{8E_C}, \quad \lambda = \frac{E_J\beta^2}{8E_C}, \quad \theta = \Phi_{\text{ext}} - \pi. \tag{S27}$$

Recall that the parameters of the bosonized lattice Hamiltonian are

$$\chi = \frac{1}{a}, \quad \mu^2 = M^2 a^2, \quad \lambda = u a^2 \exp[2\pi\Delta(a)], \tag{S28}$$

where

$$\Delta(a) = \int_{-\pi}^{\pi} \frac{d^2k}{(2\pi)^2} \frac{1}{4\sum_\mu \sin^2\left(\frac{k_\mu}{2}\right) + (Ma)^2} \tag{S29}$$

is the Feynman propagator on a lattice evaluated at the origin [S12]. Equations (S27) and (S28) together constitute a dictionary between the parameters of the bosonized massive Thirring-Schwinger model and those of the circuit-QED Hamiltonian.

B. Experimental meson–wave-packet preparation

In this section, we describe a scheme for preparing initial wave packets, focusing on meson excitations. The quarks, being topological excitations, do not couple to local operators, hence their preparation is left to future work. Our proposal goes as follows. We assume the system [i.e., Eq. (3) of the main text] is cooled down to its ground state in the confined phase. We add two ancillary qubits [S13] far away from each other. Initializing the qubits in the excited state and coupling them to the system will result in the decay of the two qubit excitations into the system, producing two wave packets of quasiparticles. Choosing a weak coupling will ensure that multi-particle states are not be excited.

To see this, first note that, in terms of the quasiparticle degrees of freedom, Eq. (S26) can be re-expressed as follows:

$$H = \sum_j \sum_k \omega_{k,j} \Psi_{k,j}^\dagger \Psi_{k,j} + \text{interactions}, \tag{S30}$$

where k is a label for the eigenstates assuming open boundary conditions. $\Psi_{k,j}^\dagger$ and $\Psi_{k,j}$ are the creation and annihilation operators for the jth meson with energy $\omega_{k,j}$, i.e.,

$$\Psi_{k,j}^\dagger |\text{vac}\rangle = |\pi_{k,j}\rangle, \tag{S31}$$

$$\Psi_{k,j} |\text{vac}\rangle = 0, \tag{S32}$$

where $|\pi_{k,j}\rangle$ are the meson quasiparticles.

Next, consider, for simplicity, a single qubit (e.g., a transmon or a fluxonium [S14]) with frequency Δ, coupled at position $i = L$. The addition to Eq. (S26) is

$$H_{\text{qubit}} = \frac{\Delta}{2}\sigma_z + g(t)\sigma_x(a_L + a_L^\dagger), \tag{S33}$$

where $a_i, a_i^\dagger = \frac{\phi_i \pm i\pi_i}{\sqrt{2}}$ are the creation and annihilation operators satisfying $[a_i, a_j^\dagger] = \delta_{ij}$, and $g(t)$ is the coupling (which can be controlled in time using a tunable coupler [S15]). In terms of mesonic quasiparticles, the entire Hamiltonian [Eq. (S26) plus Eq. (S33)] can be written as

$$H = \sum_j \sum_k \omega_{k,j} \Psi_{k,j}^\dagger \Psi_{k,j} + \sum_j \sum_k \left[g(t)\lambda_{k,j} \Psi_{k,j}^\dagger \sigma_- + \text{H.c.} \right] + \frac{\Delta}{2}\sigma_z, \tag{S34}$$

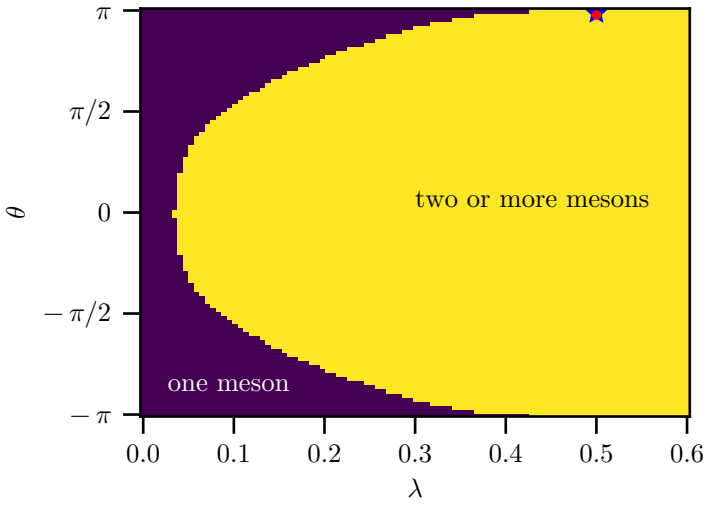

FIG. S3. Number of mesons in the confined phase. Purple (yellow) region corresponds to one (two or more) mesons. The two regions are determined by obtaining the two lowest eigenvalues above the ground state using the topologically trivial MPS quasiparticle ansatz (see Sec. III A). The single (two or more) meson region correspond to the second eigenvalue being bigger (smaller) than twice the lowest eigenvalue (mass of the fundamental meson). The remaining parameters are $\chi = 1$ and $\mu^2 = 0.1$ as in the main text. The star and circle indicate the parameters used in the main text [$\lambda = 0.5$ and $\theta = \pi - 0.04$ (star) or $\theta = \pi - 0.07$ (circle)]. The vertical axis range is $[-\pi + 0.001, \pi - 0.001]$ so as to avoid the deconfined phase at $\theta = -\pi, \pi$.

under a rotating-wave approximation (RWA) that assumes only a single excitation in the combined qubit-system and hence ignores interactions from Eq. (S30). $\lambda_{k,j} \equiv \langle \pi_{k,j} | \, a_L + a_L^\dagger \, | \text{vac} \rangle$ is a matrix element that depends on the overlaps of a_L and $a_L^\dagger$ between the vacuum $|\text{vac}\rangle$ and the meson eigenstates $|\pi_{k,j}\rangle$. Turning on $g(t)$, the (initially) excited qubit will decay into the system, producing a mesonic wave packet. The central momentum and the shape of the resulting wave packet can be controlled by choosing the qubit frequency Δ and the time dependence of the qubit-system coupling $g(t)$, as described in the Supplementary Methods of Ref. [S16]. Placing the qubit at the (left) right edge can ensure that only (right-)left-moving excitations are created. The matrix element $\lambda_{k,j}$ can either be calculated numerically or accounted for (prior to performing the actual scattering experiment) using measurements of the resulting wave-packet shape and a feedback loop. The wave-packet shape can be determined from, for example, local measurements of the density $(a_x^\dagger a_x)$ [S17] or from spectroscopic measurements of the transmitted amplitude at the other edge of the system [S18, S19].

An important subtlety is that the qubit generically couples to all mesons in the theory. If there is more than a single meson flavor, this will result in an undesired superposition of wave packets of different mesons. To mitigate this issue, this scheme can be combined with adiabatic state preparation. One can first tune the system to a parameter regime where there is only a single meson particle. A simple example is the free-boson limit with $\lambda = 0$. More generally, the "phase diagram" in Fig. S3, obtained using the uMPS methods of Sec. III A, shows the region in the $\{\lambda, \theta\}$ parameter space with only a single meson particle for $\mu^2 = 0.1$. This phase diagram is consistent with the perturbative result of Coleman [S3], predicting the existence of one meson for $|\theta| \gtrsim \pi/2$ in the limit $\lambda/\mu \to 0$ (i.e., the strong-coupling limit of the original Schwinger model). After preparing the meson wave packets in the single-meson regime, one can adiabatically tune λ and θ to their desired regime, preparing in this way the fundamental mesons of the interacting theory. Tuning both θ and λ can be accomplished using external time-dependant flux control. In order to be able to tune λ, each Josephson junction in Fig. S2 can be replaced by a SQUID, a loop composed of two junctions, realizing an effective single flux-tunable junction [S20]. Designing the two loops (the L-J loop from Fig. S2 and the SQUID loop) to be asymmetric in size allows one to control both $\lambda(\Phi_{\text{ext}})$ and $\theta(\Phi_{\text{ext}})$ with a single external flux [S18, S19, S21].

C. Generalization to 2+1D and ϕ^4 models

In this section, we provide a generalization of the circuit from Sec. II A to two spatial dimensions and discuss how it can be used to approximate other field theories such as the ϕ^4 theory. The generaelized circuit, shown in Fig. S4, consists of identical horizontal layers, each identical to Fig. S2, that are coupled vertically by additional inductors (with the same inductance L' as the horizontal coupling inductors).

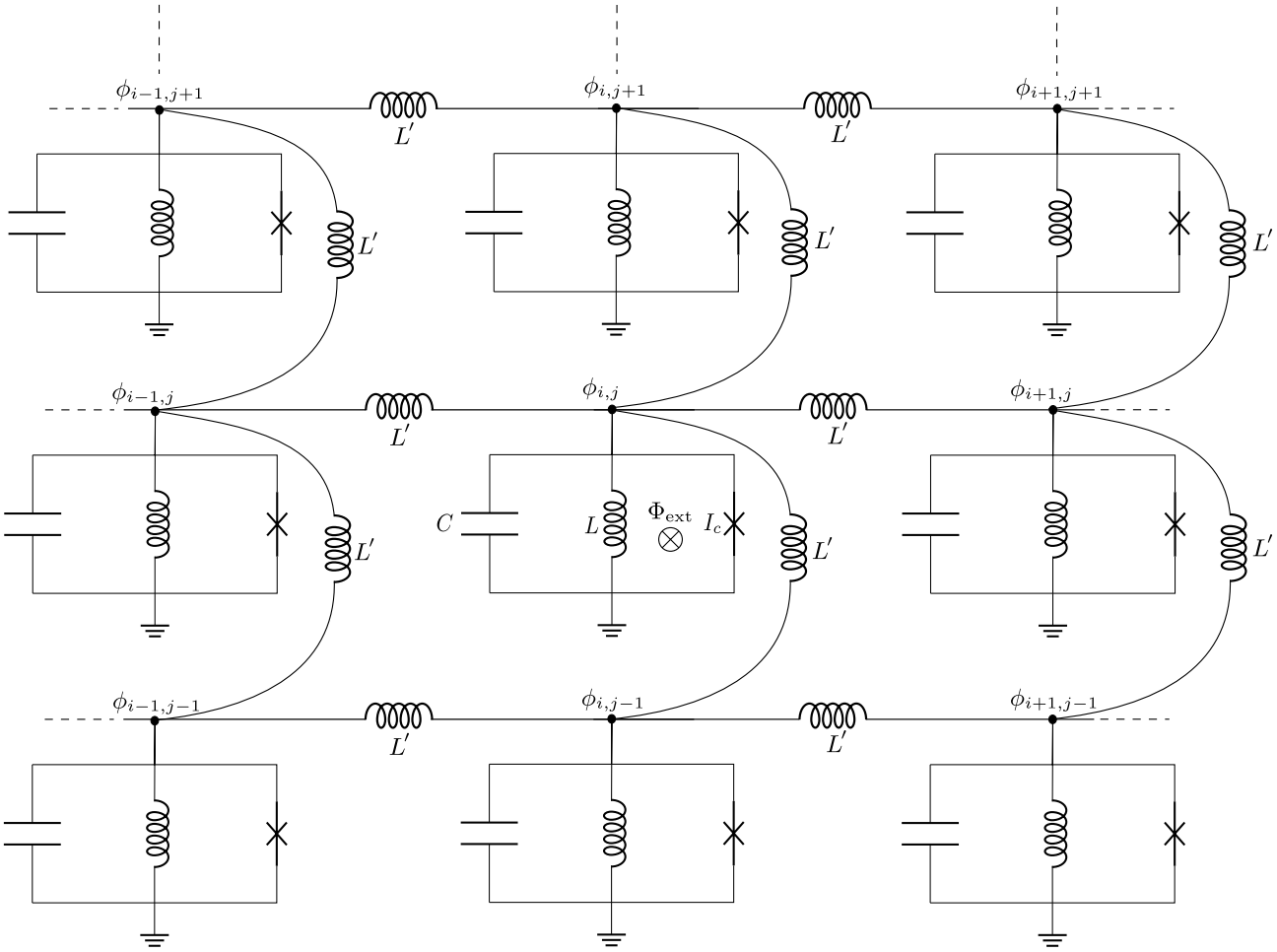

FIG. S4. Circuit diagram generalizing Fig. S2 to two spatial dimensions.

A similar derivation to the one described in Sec. II A yields the Hamiltonian

$$H = \chi \sum_{i,j} \left[\frac{\pi_{i,j}^2}{2} + \frac{(\phi_{i.j} - \phi_{i-1,j})^2 + (\phi_{i,j} - \phi_{i,j-1})^2}{2} + \frac{\mu^2 \phi_{i,j}^2}{2} - \lambda \cos(\beta \phi_{i,j} - \theta) \right], \tag{S35}$$

where i, j denote the lattice-site coordinate along the two Cartesian directions, and the parameters are the same as in Eq. (S27). This Hamiltonian may be regarded as a lattice discretization of a 2+1D massive Sine Gordon model. While this bosonic model is not dual to 2+1D QED, it can be of interest in its own right. In addition, this circuit can approximate other theories of interest. In particular, for $\theta = \pi$ and small β, we obtain an approximation of the lattice-discretized ϕ^4 model:

$$H \approx \chi \sum_{i,j} \left[\frac{\pi_{i,j}^2}{2} + \frac{(\phi_{i.j} - \phi_{i-1,j})^2 + (\phi_{i,j} - \phi_{i,j-1})^2}{2} + \frac{m^2 \phi_{i,j}^2}{2} + \frac{\tilde{\lambda}}{4!} \phi_{i,j}^4 \right], \tag{S36}$$

where $m^2 \equiv \mu^2 - \lambda\beta^2$ and $\tilde{\lambda} \equiv \lambda\beta^4$.

III. NUMERICAL METHODS

In this section, we provide more details on the uniform-matrix-product-state methods, describing the wave-packet preparation and particle detection.

A. Uniform Matrix Product States

We begin with a general review of uniform matrix product states (see Ref. [S22] for more details). A uniform matrix product state (uMPS), describing a translationally invariant state, is graphically represented as

$$|\Psi(A)\rangle = \cdots$$ 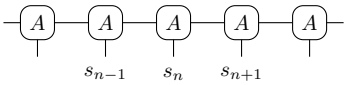 $$\cdots\,,$$ (S37)

where A^s is a $D \times D$ matrix for each basis index s. When dealing with a bosonic theory, even the local Hilbert space is infinite dimensional and needs to be truncated. For the parameters used in the main text, we found the local energy basis to be an efficient choice, i.e., the local (single-site) part of the Hamiltonian in Eq. (3) of the main text was diagonalized using a very large Fock-state basis (of ~ 2000 levels), keeping only the lowest d eigenstates (we found $d = 12$ to be sufficient for the scattering considered in the main text). The full Hamiltonian was then projected on this truncated local eigenbasis, and the ground state was subsequently found using variational methods [S23].

The quasiparticle excitations on top of the ground state can be described with the MPS quasiparticle ansatz [S9, S23, S24]

$$|\Phi_p(B)\rangle = \sum_n e^{ipn} \cdots$$ 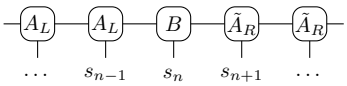 $$\cdots\,.$$ (S38)

This state is written in the so-called mixed canonical form, with the ground-state tensors A_L and $\tilde{A}_R$ in the left- and right-orthonormal forms, respectively. A_L and $\tilde{A}_R$ can either represent the same ground state for a topologically trivial excitation, in which case they are related by a gauge transformation (i.e $A_L = C^{-1}A_R C$ for a $D \times D$ matrix C), or different degenerate ground states for a topological excitation in case of a spontaneously broken symmetry. The variational optimization of the B tensor reduces to an eigenvalue problem for each $p \in [-\pi, \pi)$, providing both the dispersion relation $\mathcal{E}(p)$ and the p-dependent eigenvectors $B(p)$.

The dispersion relation is shown in Fig. S5 for the three parameter regimes studied in the main text: the deconfined phase where $\theta = \pi$, and the confined phase where $\theta = \pi - \varepsilon$ with $\varepsilon = 0.04, 0.07$. At low energies (insets), the dispersion is well approximated by the relativistic relation $\mathcal{E}(p) \approx \sqrt{m^2 + p^2}$, where m is the mass of the particle [obtained from $m \equiv \mathcal{E}(p = 0)$].

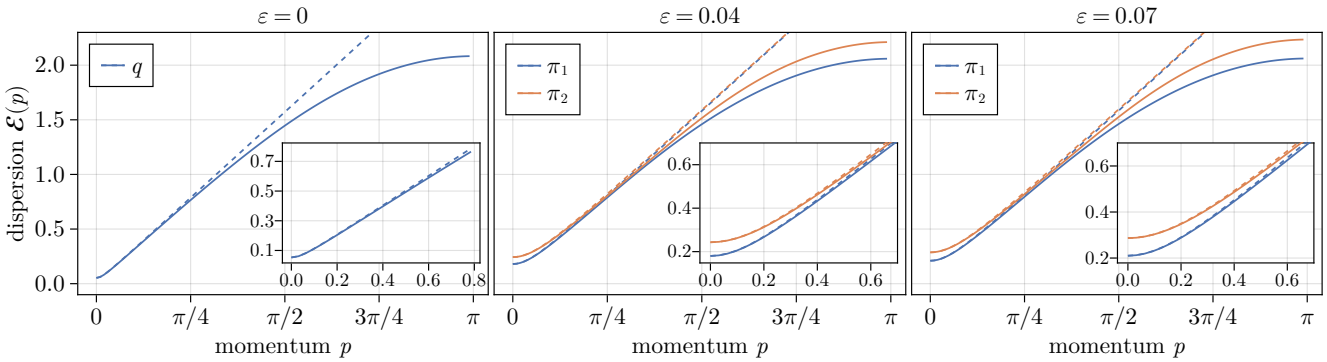

FIG. S5. Dispersion relation as a function of (positive) momentum for the three parameter regimes considered in the main text [with $\mathcal{E}(-p) = \mathcal{E}(p)$]. Solid lines are the numerical uMPS results [obtained using Eq. (S38)], and dashed lines are the relativistic approximations $\mathcal{E}(p) \approx \sqrt{m^2 + p^2}$, where m is $\mathcal{E}(p = 0)$ for the corresponding particle: quarks q in the deconfined phase ($\varepsilon = 0$) and mesons π_j in the confined phase with $\varepsilon = 0.04, 0.07$ (only the lightest two mesons corresponding to $j = 1, 2$ are shown). Insets show a zoom in the low-energy regime.

B. MPS wave-packet preparation

In this section, we describe the numerical procedure for preparing initial wave-packet states using the uMPS quasiparticles. We follow a procedure similar to the one in Refs. [S25, S26] albeit with some differences that are explained below. Using the momentum quasiparticle eigenstates in Eq. (S38), a localized wave packets can be built as

$$|\Psi_{\rm wp}\rangle = \int_{-\pi}^{\pi} dp\, c_p \, \big|\Phi_p\big(B(p)\big)\big\rangle = \sum_n \cdots$$

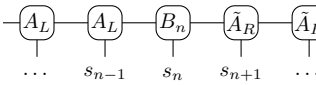

$$\cdots\,, \tag{S39}$$

where

$$B_n \equiv \int_{-\pi}^{\pi} dp\, c_p\, e^{ipn} B(p). \tag{S40}$$

Here, $c_p \sim e^{-(p-p_0)^2/(2\sigma^2)}$, which is a Gaussian function centered at p_0 with width σ. We use $\sigma = 0.12$ for the quark-antiquark wave packets (Fig. 2 of the main text) and $\sigma = 0.06$ for the meson wave packets (Fig. 3 of the main text).

As first discussed in Ref. [S25], there are several caveats with this approach. First, because the $B(p)$ tensors are determined from an eigenvalue problem for each momentum p, they come with random phases, preventing the phase coherence needed for building localized wave packets. To deal with this issue, we fix the global phase of each $B(p)$ such that one specifically chosen tensor element in each is real and positive. Second, one needs to fix the gauge redundancy of the $B(p)$ tensors (i.e., invariance of $\big|\Phi_p\big(B(p)\big)\big\rangle$ under $B^s(p) \to B^s(p) + Y\tilde{A}^s_R - e^{ip}A^s_L Y$ for any $D \times D$ matrix Y). The choices used when solving the variational minimization problem, the so-called left or right gauge fixing conditions, are inherently very asymmetric. To deal with this issue, we employ the "reflection symmetric" gauge choice of Ref. [S26] as it is applicable for both topologically trivial and nontrival excitations. Together, this approach is simpler and does not require any approximations or conditions on the wave-packets' width, unlike the methods of Refs. [S25, S26]. The final wave packet ends up slightly shifted from its intended location [which is $n = 0$ for the choice of c_p in Eq. (S40)], which can be corrected by centering it based on $\text{argmax}\|B_n\|$, as discussed in the following.

Finally, we note that, to evaluate Eq. (S40), one has to sample a finite grid of momenta p with resolution Δp, and the B_n are, therefore, periodic with period $N_p = \frac{2\pi}{\Delta p}$, i.e., $B_{n+N_p} = B_n$. We choose N_p large enough so that the wave packet comfortably fits inside a single period (we used $N_p = 400$), which we take to be centered around $n^* = \text{argmax}\|B_n\|$. Of this N_p-sized interval of B_n tensors, we only keep $N < N_p$ tensors that satisfy $\|B_n\|/\|B_{n^*}\| \geq \epsilon$ for some chosen threshold ϵ (we used $\epsilon = 10^{-3}$), which we label by $n \in [i+1, i+N]$ for a chosen i along the uMPS chain. The integral in Eq. (S39) becomes a finite sum and can be analytically expressed as

$$|\Psi_{\rm wp}\rangle = \cdots$$

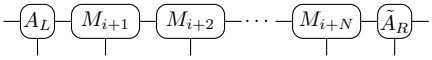

$$\cdots\,,$$

$$M_{i+1} = \begin{pmatrix} A_L & B_{i+1} \end{pmatrix}, \quad M_{n\in[i+2,i+N-1]} = \begin{pmatrix} A_L & B_n \\ 0 & \tilde{A}_R \end{pmatrix}, \quad M_{i+N} = \begin{pmatrix} B_{i+N} \\ \tilde{A}_R \end{pmatrix}. \tag{S41}$$

To create the initial two-particle state, this procedure can be carried out twice to create two wave packets with opposite momenta. Given that A_L is related to A_R by a gauge transformation, i.e., $A_L C = C A_R$, the states are then glued together using the matrix C^{-1}. The result is a nonuniform window of tensors surrounded by the uniform ground state. Note that the bond dimension of the tensors in Eq. (S41) is not uniform, as some have the value D and others $2D$. Finally, the one-site time-dependent variational principle (TDVP) [S27] is used to evolve the state in time, which does not change the bond dimensions. Hence, prior to the time-evolution, we expand the bond dimensions of all the tensors to a uniform value $D' \geq 2D$. For the quark-antiquark scattering (Fig. 2 of the main text), we found that $D = 20$ and $D' = 50$ were sufficient for convergence at late times, while the meson-meson scattering in the confined phase required a larger bond dimension ($D = 40$ and $D' = 100$). During the time evolution, we only update the tensors inside the nonuniform window [S28–S30]. To decide whether to extend the window, at each time step, we compute the entanglement entropy across the bonds at the edges of the window and compare that to the entropy of the vacuum, extending the window by a site if the relative difference is greater than a specified threshold (which we chose to be 0.02).

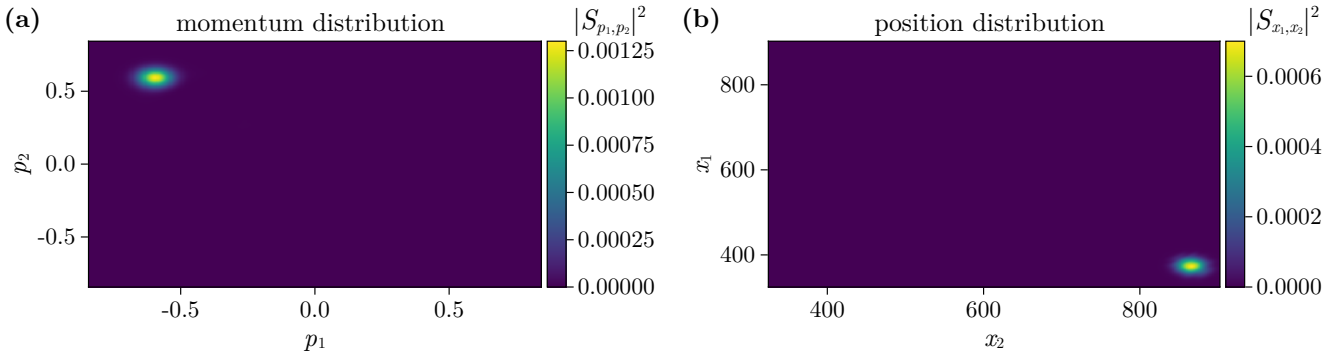

FIG. S6. (a) Momentum and (b) position probability distributions of observing a $\pi_1\pi_1$ meson pair at $t = 345$ following the $\pi_1\pi_1$ collision at $\varepsilon = 0.07$ in Fig. 3 of the main text.

C. Particle detection

In this section, we describe how the scattering matrix can be computed by projecting on multi-particle basis states. As long as the particles are well separated, one can use Eq. (S38) to build multi-particle states, akin to the asymptotic "out" states in the definition of the S-matrix. For example, a two-particles state, with a particle on the left with momentum p_1 and a particle on the right with momentum p_2, is expressed as

$$|\Phi_{p_1,p_2}\rangle = \sum_{n_1\in W_L}\sum_{n_2\in W_R} e^{ik_1n_1}e^{ik_2n_2}\cdots - A_L - B(p_1) - \tilde{A}_R - \cdots - C^{-1} - \tilde{A}_L - B(p_2) - A_R - \cdots . \tag{S42}$$

The sums are restricted such that the two excitation tensors B appear in disjoint regions W_L and W_R and are separated by some minimum number r of vacuum tensors, ensuring that there are no interactions between the particles (we found $r = 40$ to be sufficient for both meson and quark scattering in the main text). Moreover, since we are projecting on a time-evolved state where the particles are constrained to a finite window of the uMPS, we further restrict the sums to the sites within this nonuniform window. Using the left gauge-fixing condition for the left-most B tensor, and the right gauge-fixing condition for the right-most B tensor [S22], ensures that overlaps where either of the B tensors is outside of the window are exactly zero. The finite sums in Eq. (S42) can then be summed exactly and expressed as a single MPS, similarly to Eq. (S41).

To compute the full n-particle momentum distribution (for $n = 2$, $S_{p_1,p_2} \equiv \langle\Phi_{p_1,p_2}|\psi(t)\rangle$, where $|\psi(t)\rangle$ is the time-evolved state), M_p^n contractions need to be performed, where M_p is the desired number of p samples (i.e., the equivalent of N_p in the incoming wave-packet construction). This can be sped up by precomputing partial contractions. For example, for the two-particle case, we compute the partial left and right contractions for each value of p, which scale as $\sim M_p|W_L|$ and $\sim M_p|W_R|$, respectively. Then, the $\sim M_p^2$ contractions are very efficient since the remaining tensor network is of length ~ 1. As an example, Fig. S6 depicts the result of projecting the state following the meson-meson collision (this process is depicted in Fig. 3 of the main text) on the lightest meson-meson ($\pi_1\pi_1$) two-particle basis. From the momentum distribution, the position distribution (S_{x_1,x_2}) is computed by a Fourier transform. For this to work, it is crucial that the phases of the $B(p)$ tensors are fixed prior to the projection, as described in Sec. III B. To avoid multiple unphysical copies due to the periodicity of the discrete Fourier transform, we choose the number of p samples, M_p, to be larger than the window size (we used $M_p = 400$ for the quark-antiquark scattering and $M_p = 1300$ for the meson-meson scattering). Finally, fitting Gaussians to the marginals of these distributions produces the information plotted in Fig. 3(c) of the main text.

[S1] J. Fröhlich and E. Seiler, The massive Thirring-Schwinger model (QED_2) : Convergence of perturbation theory and particle structure, Helvetica Phys. Acta **49**, 889 (1976).
[S2] S. Coleman, Quantum sine-Gordon equation as the massive Thirring model, Phys. Rev. D **11**, 2088 (1975).
[S3] S. Coleman, More about the massive Schwinger model, Ann. Phys. **101**, 239 (1976).

[S4] S. Coleman, R. Jackiw, and L. Susskind, Charge shielding and quark confinement in the massive schwinger model, Ann. Phys. **93**, 267 (1975).

[S5] Recall that we have restricted the model to the net zero electric-charge sector.

[S6] R. F. Dashen, B. Hasslacher, and A. Neveu, Particle spectrum in model field theories from semiclassical functional integral techniques, Phys. Rev. D **11**, 3424 (1975).

[S7] A. B. Zamolodchikov and A. B. Zamolodchikov, Factorized S-matrices in two dimensions as the exact solutions of certain relativistic quantum field theory models, Ann. Phys. **120**, 253 (1979).

[S8] D. J. Griffiths and D. F. Schroeter, *Introduction to Quantum Mechanics*, third edition ed. (Cambridge University Press, Cambridge ; New York, NY, 2018).

[S9] J. Haegeman, S. Michalakis, B. Nachtergaele, T. J. Osborne, N. Schuch, and F. Verstraete, Elementary Excitations in Gapped Quantum Spin Systems, Phys. Rev. Lett. **111**, 080401 (2013).

[S10] M. Peruzzo, F. Hassani, G. Szep, A. Trioni, E. Redchenko, M. Žemlička, and J. M. Fink, Geometric Superinductance Qubits: Controlling Phase Delocalization across a Single Josephson Junction, PRX Quantum **2**, 040341 (2021).

[S11] We work in units where $\hbar = 1$ and the reduced flux quantum $\Phi_0/2\pi = \hbar/(4e^2) = 1$. This e is not to be confused with the e of the Schwinger model.

[S12] H. Ohata, Monte Carlo study of Schwinger model without the sign problem, arXiv:2303.05481.

[S13] S. P. Jordan, K. S. Lee, and J. Preskill, Quantum algorithms for quantum field theories, Science **336**, 1130 (2012).

[S14] I. Siddiqi, Engineering high-coherence superconducting qubits, Nat Rev Mater **6**, 875 (2021).

[S15] S. E. Rasmussen, K. S. Christensen, S. P. Pedersen, L. B. Kristensen, T. Baekkegaard, N. J. S. Loft, and N. T. Zinner, Superconducting Circuit Companion-an Introduction with Worked Examples, Phys. Rev. Appl. **10**, 40204 (2021).

[S16] N. Y. Yao, C. R. Laumann, A. V. Gorshkov, H. Weimer, L. Jiang, J. I. Cirac, P. Zoller, and M. D. Lukin, Topologically protected quantum state transfer in a chiral spin liquid, Nat Commun **4**, 1585 (2013).

[S17] X. Zhang, E. Kim, D. K. Mark, S. Choi, and O. Painter, A superconducting quantum simulator based on a photonic-bandgap metamaterial, Science **379**, 278 (2023).

[S18] P. Forn-Díaz, J. J. García-Ripoll, B. Peropadre, J.-L. Orgiazzi, M. A. Yurtalan, R. Belyansky, C. M. Wilson, and A. Lupascu, Ultrastrong coupling of a single artificial atom to an electromagnetic continuum in the nonperturbative regime, Nature Phys **13**, 39 (2017).

[S19] A. Vrajitoarea, R. Belyansky, R. Lundgren, S. Whitsitt, A. V. Gorshkov, and A. A. Houck, Ultrastrong light-matter interaction in a photonic crystal, arXiv:2209.14972.

[S20] A. Blais, A. L. Grimsmo, S. M. Girvin, and A. Wallraff, Circuit Quantum Electrodynamics, Rev. Mod. Phys. **93**, 025005 (2021).

[S21] L. Magazzù, P. Forn-Díaz, R. Belyansky, J.-L. Orgiazzi, M. A. Yurtalan, M. R. Otto, A. Lupascu, C. M. Wilson, and M. Grifoni, Probing the strongly driven spin-boson model in a superconducting quantum circuit, Nat Commun **9**, 1403 (2018).

[S22] L. Vanderstraeten, J. Haegeman, and F. Verstraete, Tangent-space methods for uniform matrix product states, SciPost Phys. Lect. Notes , 7 (2019).

[S23] V. Zauner-Stauber, L. Vanderstraeten, M. T. Fishman, F. Verstraete, and J. Haegeman, Variational optimization algorithms for uniform matrix product states, Phys. Rev. B **97**, 045145 (2018).

[S24] J. Haegeman, B. Pirvu, D. J. Weir, J. I. Cirac, T. J. Osborne, H. Verschelde, and F. Verstraete, Variational matrix product ansatz for dispersion relations, Phys. Rev. B **85**, 100408 (2012).

[S25] M. Van Damme, L. Vanderstraeten, J. De Nardis, J. Haegeman, and F. Verstraete, Real-time scattering of interacting quasiparticles in quantum spin chains, Phys. Rev. Res. **3**, 013078 (2021).

[S26] A. Milsted, J. Liu, J. Preskill, and G. Vidal, Collisions of False-Vacuum Bubble Walls in a Quantum Spin Chain, PRX Quantum **3**, 020316 (2022).

[S27] J. Haegeman, C. Lubich, I. Oseledets, B. Vandereycken, and F. Verstraete, Unifying time evolution and optimization with matrix product states, Phys. Rev. B **94**, 165116 (2016).

[S28] A. Milsted, J. Haegeman, T. J. Osborne, and F. Verstraete, Variational matrix product ansatz for nonuniform dynamics in the thermodynamic limit, Phys. Rev. B **88**, 155116 (2013).

[S29] H. N. Phien, G. Vidal, and I. P. McCulloch, Dynamical windows for real-time evolution with matrix product states, Phys. Rev. B **88**, 035103 (2013).

[S30] V. Zauner, M. Ganahl, H. G. Evertz, and T. Nishino, Time Evolution within a Comoving Window: Scaling of signal fronts and magnetization plateaus after a local quench in quantum spin chains, J. Phys.: Condens. Matter **27**, 425602 (2015).